

See discussions, stats, and author profiles for this publication at: <https://www.researchgate.net/publication/233381377>

Bimagnetic CoO Core/CoFe₂O₄ Shell Nanoparticles: Synthesis and Magnetic Properties

ARTICLE *in* CHEMISTRY OF MATERIALS · FEBRUARY 2012

Impact Factor: 8.35 · DOI: 10.1021/cm2028959

CITATIONS

18

READS

104

7 AUTHORS, INCLUDING:



Enio Lima

Centro Atómico Bariloche

43 PUBLICATIONS 465 CITATIONS

[SEE PROFILE](#)



Elin Lilian Winkler

Centro Atómico Bariloche

56 PUBLICATIONS 813 CITATIONS

[SEE PROFILE](#)



Dina Tobia

Centro Atómico Bariloche

18 PUBLICATIONS 195 CITATIONS

[SEE PROFILE](#)



Elisabetta Agostinelli

Italian National Research Council

86 PUBLICATIONS 673 CITATIONS

[SEE PROFILE](#)

Bimagnetic CoO Core/CoFe₂O₄ Shell Nanoparticles: Synthesis and Magnetic Properties

Enio Lima, Jr., ^{†,‡} Elin L. Winkler, ^{*,†,‡} Dina Tobia, ^{†,‡} Horacio E. Troiani, [†] Roberto D. Zysler, ^{†,‡} Elisabetta Agostinelli, ^{¶,‡} and Dino Fiorani ^{¶,‡}

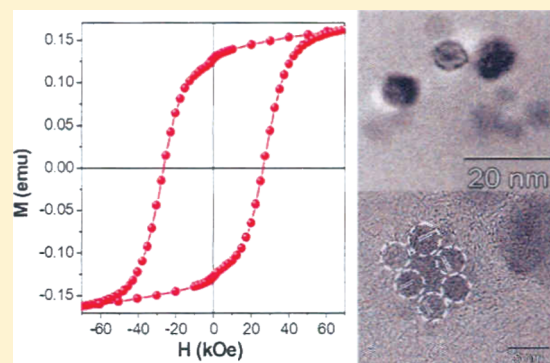
[†]Centro Atómico Bariloche, CNEA-CONICET, 8400 S.C. de Bariloche, Río Negro, Argentina

[‡]Argentine-Italian Joint Laboratory of Nanomagnetism, LIANAM, Laboratorio Resonancias Magnéticas –CNEA / Istituto di Struttura della Materia – CNR

[¶]Istituto di Struttura della Materia, CNR, Area della Ricerca di Roma, C.P. 10, I-00016 Monterotondo Staz., Rome, Italy

ABSTRACT: In this work we report on the synthesis, the microstructural characterization, and the magnetic properties of ~7 nm bimagnetic core/shell nanoparticles prepared by seed-mediated growth high temperature decomposition of organometallic precursor. The nanoparticles are formed by an antiferromagnetic CoO core coated with ferromagnetic CoFe₂O₄ shell of 2–3 nm of thickness. XRD and electron diffraction patterns show the reflections of the structure of the CoFe₂O₄ and CoO phases and Dark- and Bright-field TEM images provide evidence of the core–shell morphology of the system. Magnetic measurements show that the system presents a remarkably large coercivity and high squareness (at 5 K, H_C = 27.8 kOe and M_r/M_S = 0.79), compared to CoFe₂O₄ single phase nanoparticles of comparable size. The enhancement of the effective anisotropy is attributed to the surface and interface exchange coupling effects.

KEYWORDS: bimagnetic nanoparticles, CoO/CoFe₂O₄ nanoparticles, interface exchange coupling, magnetic anisotropy



INTRODUCTION

Magnetic nanoparticles have been widely investigated for their novel properties as well as for their numerous applications in different technological fields¹ and in biomedicine.² Many technological devices, e.g. magnetic storage media and permanent magnets, require high stability of the magnetization. However, further size reduction of single phase nanoparticles has to face the so-called “superparamagnetic limit”, which imposes a lower threshold in the grain size to maintain thermal stability of the magnetization, thus limiting the development of miniaturized devices.³ Recently, Skumryev et al.⁴ have shown that the superparamagnetic threshold can be pushed to a lower grain size in nanostructures with ferromagnetic (FM)/antiferromagnetic (AFM) interface. This was achieved exploiting the interface exchange coupling for increasing the effective magnetic anisotropy of the system.^{4–6} The possibility of tuning the magnetic anisotropy through interface exchange coupling between materials with different magnetic structures and different magnetic anisotropies has driven in the last years the research on bimagnetic core/shell nanoparticles. In this frame, new size-controlled synthesis methods were developed.^{7–10} Among them the high temperature decomposition of organometallic precursor deserves special attention as this method not only allows the fabrication of monodispersed nanoparticles^{7–11} but also makes it possible to prepare high-quality bimagnetic core/shell nanoparticles by seed-mediated

growth.^{12–17} Within this picture, the motivation of this work is the fabrication of bimagnetic AFM-core/ferrimagnetic (FiM)-shell nanoparticles and the investigation of the magnetic properties with special interest toward the anisotropy enhancement with respect to the single phase counterparts. It is well-known that the CoFe₂O₄ spinel oxide is a hard magnetic material with large coercivity and magnetization, making it an excellent candidate for technological applications. Its coercivity and squareness (defined as the remanence (M_r) normalized to the saturation magnetization (M_S), M_r/M_S) is strongly size dependent.^{18,19} Chinnasamy and co-workers found that for CoFe₂O₄ particles the maximum value of the coercivity, H_C ~ 20 kOe, is reached for an average diameter of <math>\langle \phi \rangle = 40\text{ nm}. Then the coercivity decreases to H_C ~ 10 kOe when the size is reduced down to <math>\langle \phi \rangle = 8\text{ nm}. We have prepared core/shell systems with the aim of improving the magnetic stability of CoFe₂O₄ at nanometer scale. In particular, in the present work, we report the synthesis, the microstructural characterization, and an investigation of the magnetic properties of CoO AFM nanoparticles coated with CoFe₂O₄ FiM shell. The results show an enhancement of the effective anisotropy with respect to the single phase CoFe₂O₄ nanoparticles.

Received: September 27, 2011

Revised: December 21, 2011

Published: December 21, 2011

■ EXPERIMENTAL SECTION

$\text{CoO}/\text{CoFe}_2\text{O}_4$ nanoparticles with molar ratio 3:1 were synthesized by high-temperature decomposition of organometallic precursors followed by seed mediated grown shell. First, monodispersed CoO nanoparticles were prepared by mixing 3 mmol $\text{Co}(\text{II})$ acetylacetone ($\text{Co}(\text{acac})_2$) with long-chain alcohol 1–2 octanediol (2×10^{-2} mmol), diphenyl ether (solvent, 189 mmol), surfactants oleic acid (6 mmol), and oleylamine (6 mmol). The preparation was magnetically stirred and heated to reflux up to $T \sim 260^\circ\text{C}$ for 120 min. Then the mixture was cooled down to room temperature, and the precursors were added to overgrow with CoFe_2O_4 . In this step $\text{Co}(\text{acac})_2$ and $\text{Fe}(\text{acac})_3$ were added with the 1:2 molar ratio (0.6:1.2 mmol) together with 1–2 octanediol (2×10^{-2} mmol), diphenyl ether (189 mmol), and surfactants oleic acid and oleylamine (3 mmol of each one). The preparation was magnetically stirred and heated up to the boiling temperature $T \sim 260^\circ\text{C}$ for another 120 min. After cooling down to room temperature the nanoparticles were precipitated by centrifugation (14000 rpm/30 min.) and washed with a mix of ethanol and toluene 10:1 solution. In order to improve the sample crystallinity the obtained dry powder was annealed at $T = 300^\circ\text{C}$ in air atmosphere for two hours. The structural characterization was performed by X-ray powder diffraction (XRD) in a Philips PW3020 diffractometer with $\text{Cu K}\alpha$ radiation, using ground glass slides as sample holders. The morphology and particle size distribution were determined from transmission electron microscopy (TEM) images obtained in a Philips CM200 UT microscope operating at 200 kV. In order to avoid the mechanical movement of the system, the magnetic measurements were carried out on nanoparticles dispersed into diamagnetic epoxy samples. The measurements were taken using a superconducting quantum interference device (SQUID, Quantum Design) magnetometer with 70 kOe maximum field.

■ RESULTS AND DISCUSSION

Structural and Morphological Characterization. Figure 1 shows the typical XRD pattern of the $\text{CoO}/\text{CoFe}_2\text{O}_4$

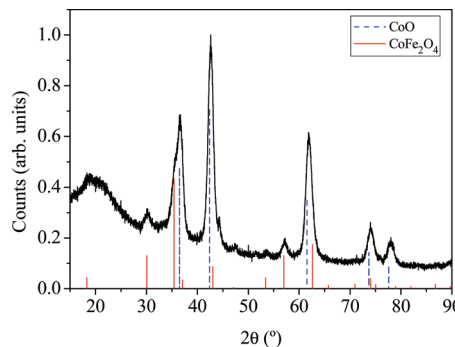


Figure 1. XRD pattern of the $\text{CoO}/\text{CoFe}_2\text{O}_4$ nanoparticles. The figure also includes the (hkl) Bragg diffraction position for the Fm3m CoO phase and the Fd3m (JCPDS-ICCD Card #43-1004) CoFe_2O_4 phases (JCPDS-ICCD Card #22-1086).

nanoparticles system. This figure also includes the (hkl) Bragg diffraction positions for the Fm3m CoO phase (JCPDS-ICCD Card #43-1004) and the Fd3m CoFe_2O_4 (JCPDS-ICCD Card #22-1086) phase. As shown in the figure, the position and the relative intensity match well with the structure of the two phases. The XRD diffraction peaks are quite broad, due to the nanometric size of the particles. The crystallite size can be estimated from the linewidth using the Scherrer equation.²⁰ The average diameter of the CoO particles is $\langle\phi\rangle = 6$ nm, estimated from the (200) ($\sim 42.6^\circ$) peak, and the average size of CoFe_2O_4 phase is 7 nm, estimated from the (511) ($\sim 57^\circ$) peak.

The morphology of the nanoparticles is shown by the TEM image in Figure 2-a. The inset shows the nanoparticles size distribution, where the average diameter $\langle\phi\rangle = 7$ nm with $\sigma = 2$ nm were obtained using a Gaussian fit. Figure 2-b shows the electron diffraction pattern: the ring pattern is in agreement with the diffraction of the standard Fm3m CoO and the Fd3m CoFe_2O_4 bulk phases; the brighter rings correspond to the electron diffraction of the CoO phase.

At higher TEM magnification nanostructure details are clearly observed. Figure 3 shows that the cobalt ferrite shell is polycrystalline, as was noticed in other core/shell and hollow nanoparticles.^{21,22} However, as the CoO -core is a seed for the CoFe_2O_4 crystallite nucleation, the shell nanocrystals grow up with a preferential orientation (see Figure 3). In addition it is worth noting that the TEM image is a two-dimensional projection of a three-dimensional structure, as a consequence while the TEM image depicts the shell thickness, the XRD sense the nanograins volume. This fact explains the bigger CoFe_2O_4 crystallite size obtained from the X-ray diffraction linewidth. From TEM images, the interplanar distance $d = 3.0$ (2) Å is measured, which matches well with the interplanar distance of the (220) plane of the CoFe_2O_4 phase ($d = 2.968$ Å), which is shown in Figure 3b. The core/shell structure was also observed by high resolution dark field image recorded using a small objective aperture positioned on a section of the (111) CoFe_2O_4 diffraction ring. In this way the nanoparticle shell shows a big contrast indicating that it is composed by the CoFe_2O_4 spinel phase (Figure 3 (c)).

Magnetic Properties. The temperature dependence of the zero field cooling (ZFC) and field cooling (FC) magnetization curves present an irreversible behavior up to the highest measured temperature (Figure 4). At low temperature, the FC magnetization curve shows an almost flat behavior, which evidences significant magnetic interaction effects. As the nanoparticles were dispersed in a nonmagnetic epoxy we ascribe this behavior to magnetic interaction within the nanoparticles.^{22,23} In addition, the ZFC-magnetization curve presents a kink around $T \sim 307$ K. This anomaly is evidenced in the inset of Figure 4, where the ZFC magnetization derivative versus temperature is plotted showing a maximum at $T \sim 307$ K. It is related to the CoO Néel temperature, which is $T_{N-\text{Bulk}} = 293$ K^{24,25} in the bulk state. Such increase of T_N with respect to the bulk value behavior has been also observed in other AFM^{13,26} and FiM nanoparticles systems.^{27–29} The origin of the T_N enhancement is debated, and it was attributed to different factors, e.g. the change in the dimensionality,^{26,27} surface and interface exchange coupling effects, enhancement of the surface exchange interaction due to the surface disorder;^{28–30} in ferrite nanoparticles the higher T_N values were ascribed to the increase of the superexchange interaction due to the cation disorder that increases the superexchange bond angle.^{29,28}

Hysteresis cycles measured at different temperatures are shown in Figure 5. It is worth noting the remarkably large coercivity and high squareness: at $T = 5$ K, $H_C = 27.8$ kOe and $M_r/M_S = 0.79$ with respect to the single phase CoFe_2O_4 counterpart. In CoFe_2O_4 -core/ MnO -shell¹² of $\phi \sim 8$ nm system the coercive field at 10 K is much smaller of $H_C \sim 2.6$ kOe. In this case, the reduction of H_C was ascribed to cation mixing between the core and shell resulting in a softer Mn-substituted CoFe_2O_4 spinel. The hysteresis cycle, measured at 10 K, of ~ 5 nm CoFe_2O_4 single phase nanoparticles (prepared by the same route³¹) is reported in Figure 6 together with that

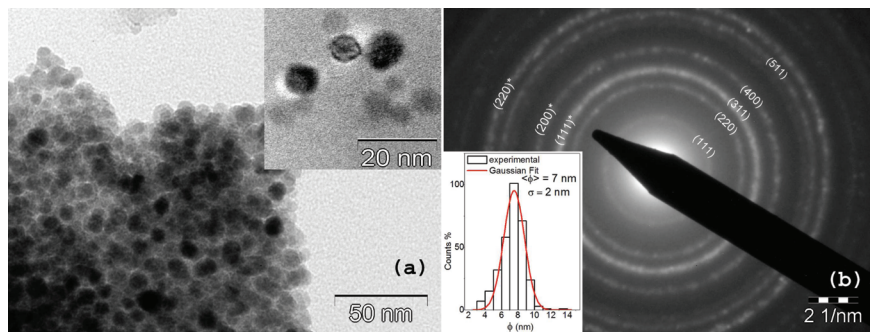


Figure 2. a) TEM image of the CoO/CoFe₂O₄ nanoparticles. The inset in the image shows a highly magnified portion. b) Electron diffraction pattern of the nanoparticle system. The ring pattern is indexed with the standard Fm3m CoO (signaled with * at the image) and the Fd3m CoFe₂O₄ phases. The inset in the image in part b shows a particle size distribution histogram.

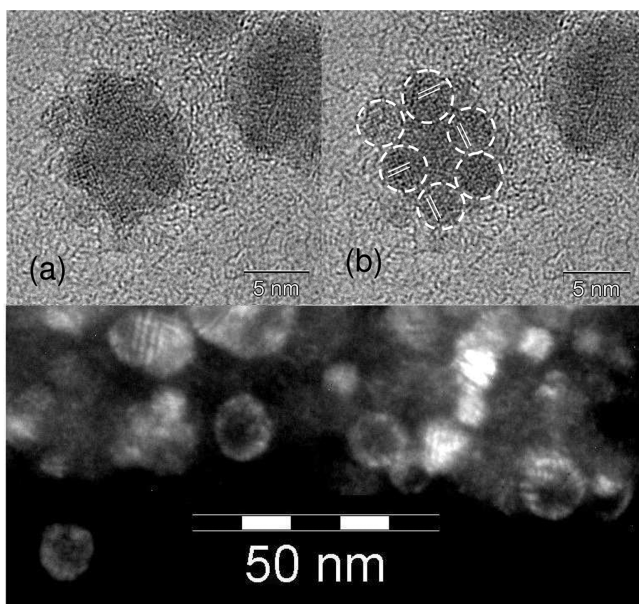


Figure 3. a) High resolution TEM image. (b) Notice that the surface is formed by small single crystals of 2–3 nm of diameter. The observed interplanar distance is $d = 3.0$ (2) Å which matches well with the interplanar distance of the (220) plane of the CoFe₂O₄ phase ($d = 2.968$ Å). c) High resolution dark field image recorded using a small objective aperture positioned on a section of the (111) CoFe₂O₄ diffraction ring, the bright contrast corresponds to the CoFe₂O₄ spinel phase.

of the bimagnetic system, for comparison. The temperature dependence of H_C and M_r/M_S is reported in Figure 7 for both systems, showing in all the temperature range a larger hardness for the core/shell sample. This is attributed to the strong interface exchange coupling between the FiM and the AFM phases (exchange anisotropy).

No shift of the magnetization cycle after field cooling ($H_{cooling} = 50$ kOe) from $T = 350$ K was observed. The lack of Exchange Bias (EB) effect is not unexpected. The prerequisite for the observation of EB is that magnetic anisotropy energy of the AFM phase is larger than the interface exchange energy. Indeed, only if such requirement is satisfied, the AFM phase can exert a pinning action on the magnetization of the FM (FiM) phase.³² Moreover, the anisotropy of the AFM phases has to be much larger than that of the FM (FiM) phase.

In the CoO/CoFe₂O₄ system, both the AFM and FiM bulk phases have high anisotropy. The tabulated magnetocrystalline

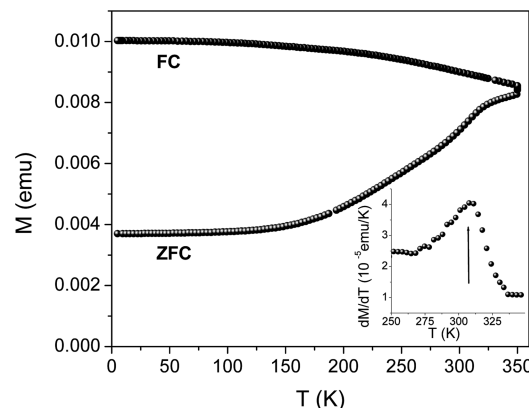


Figure 4. Temperature dependence of the zero field cooling (ZFC) and field cooling (FC) magnetization curves. Inset: ZFC magnetization derivate.

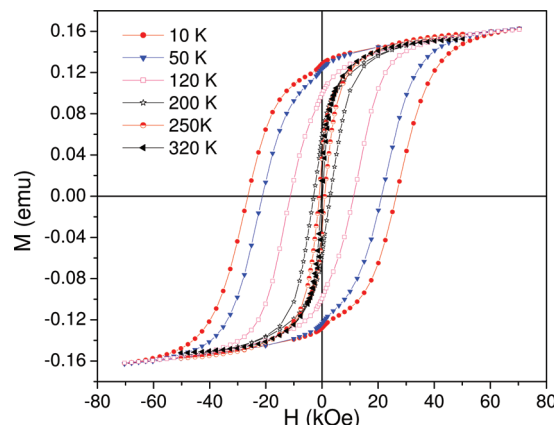


Figure 5. Hysteresis cycles at different temperatures.

bulk anisotropy of the CoFe₂O₄ phase is $K \sim 4 \times 10^6$ erg/cm³. On the other hand, the magnetic anisotropy of the AFM oxide is not well determined because it is difficult to prepare and measure a single domain sample; for this reason, there is a wide dispersion of the K-value for CoO. Moreover, it is well-known that in the CoO the spins can be rotated more easily in the (111) plane than out of plane; this fact defines two magnetic anisotropy constants K_1 and K_2 for the rotation out of plane and in-plane, respectively. Kanamori³³ has calculated $K_1 \sim 2.7 \times 10^8$ erg/cm³. From torque measurements Meiklejohn and Bean³⁴ estimated for CoO powder an effective anisotropy value of $K \sim 5 \times 10^6$ erg/cm³ at 77 K. Recently, Tracy and co-

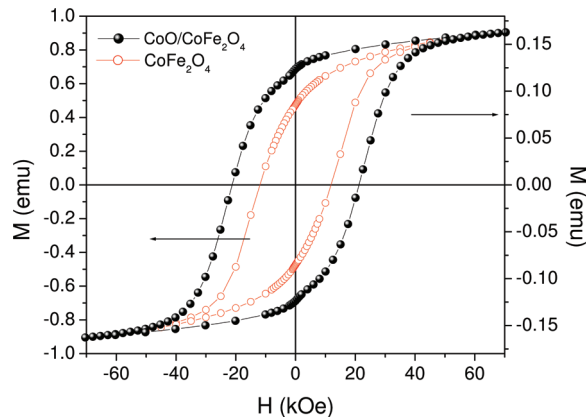


Figure 6. Hysteresis cycles at 10 K for ~ 5 nm CoFe_2O_4 single phase nanoparticles and $\text{CoO}/\text{CoFe}_2\text{O}_4$ core/shell nanoparticles.

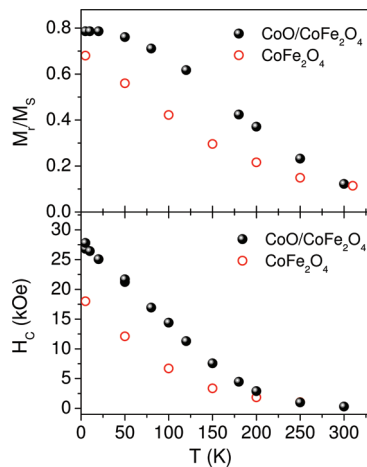


Figure 7. Temperature dependence of H_C and M_r/M_S , for the single CoFe_2O_4 phase nanoparticles and the bimagnetic $\text{CoO}/\text{CoFe}_2\text{O}_4$ system.

workers³⁵ have determined from magnetization measurements for CoO grains of ~ 3 nm an effective magnetic anisotropy of $K \geq 3 \times 10^7$ erg/cm³. However, since the anisotropy is strongly particle size, shape, and surface effects dependent, it is difficult to predict the effective anisotropies of the two phases in our core/shell system. The surface and interface effects (increase of anisotropy due to interface exchange coupling) are expected to be very important for the very thin CoFe_2O_4 shell, enhancing the magnetic anisotropy. The lack of EB would indicate that the two phases are very strongly exchange coupled and that the effective anisotropy of the CoFe_2O_4 phase is larger than that of CoO phase.

CONCLUSIONS

In conclusion, we have reported the synthesis, the microstructural characterization, and an investigation of the magnetic properties of ~ 7 nm bimagnetic core/shell nanoparticles. The nanoparticles are formed by an AFM CoO core coated by a FM CoFe_2O_4 shell of 2–3 nm of thickness. We have found that the system presents a remarkably large coercivity and high squareness reaching, at 5 K, $H_C = 27.8$ kOe and $M_r/M_S = 0.79$. The increase of the effective magnetic anisotropy of the core/shell system with respect to that of ~ 5 nm CoFe_2O_4 single phase nanoparticles ($H_C = 18$ kOe and $M_r/M_S = 0.68$ at 5 K)

can be explained by the surface and strong interface exchange coupling effects.

AUTHOR INFORMATION

Corresponding Author

*Phone: +54 (294) 4445158. Fax: +54 (294) 4445299. E-mail: winkler@cab.cnea.gov.ar.

ACKNOWLEDGMENTS

The authors thank ANPCyT Argentina through Grant Nos. PICTs 2007-832, CONICET Argentina through Grant No. PIP 200801-01333, and U. N. Cuyo through Grant No. 06/C334.

REFERENCES

- (1) Schmid, G. *Nanoparticles: From Theory to Applications*; Wiley-VCH: 2004.
- (2) Tartaj, P.; Morales, M. P.; Verdaguer, S. V.; Carreño, T. G.; Serna, C. G. *J. Phys. D: Appl. Phys.* **2003**, *36*, R182, and references therein.
- (3) O'Handley, R. C. *Modern Magnetic Materials*; Wiley and Sons: New York, 2000.
- (4) Skumryev, V.; Stoyanov, S.; Zhang, Y.; Hadjipanayis, G.; Givord, D.; Nogués, J. *Nature (London)* **2003**, *423*, 850.
- (5) Meiklejohn, W. H.; Bean, C. P. *Phys. Rev. B* **1956**, *102*, 1413.
- (6) Berkowitz, A. E.; Takano, K. *J. Magn. Magn. Mater.* **1999**, *200*, S52.
- (7) Sun, S.; Zeng, H. *J. Am. Chem. Soc.* **2002**, *124*, 8204.
- (8) Sun, S.; Zeng, H.; Robinson, D. R.; Raoux, S.; Rice, P. M.; Wang, S. X.; Li, G. *J. Am. Chem. Soc.* **2004**, *126*, 273.
- (9) Zeng, H.; Rice, P. M.; Wang, S. X.; Sun, S. *J. Am. Chem. Soc.* **2004**, *126*, 11458.
- (10) Elkins, K. E.; Vedantam, T. S.; Liu, J. P.; Zeng, H.; Sun, S.; Ding, Y.; Wang, Z. L. *Nano Lett.* **2003**, Vol. 3, 1647.
- (11) Lima, E. Jr.; De Biasi, E.; Vasquez Mansilla, M.; Saleta, M. E.; Effenberg, F.; Rossi, L. M.; Cohen, R.; Rechenberg, H. R.; Zysler, R. D. *J. Appl. Phys.* **2010**, *108*, 103919.
- (12) Masala, O.; Seshadri, R. *J. Am. Chem. Soc.* **2005**, *127*, 9354.
- (13) López-Ortega, A.; Tobía, D.; Winkler, E.; Golosovsky, I. V.; Salazar-Alvarez, G.; Estrade, S.; Estrader, M.; Sort, J.; González, M. A.; Suriñach, S.; Arbiol, J.; Peiró, F.; Zysler, R. D.; Baró, M. D.; Nogués, J. *J. Am. Chem. Soc.* **2010**, *132*, 9398.
- (14) Kim, H.; Achermann, M.; Balet, L. P.; Hollingsworth, J. A.; Klimov, V. I. *J. Am. Chem. Soc.* **2005**, *127*, 544.
- (15) Zeng, H.; Sun, S.; Li, J.; Wang, Z. L.; Liu, J. P. *Appl. Phys. Lett.* **2004**, *85*, 792.
- (16) Cannas, C.; Musinu, A.; Ardu, A.; Orrú, F.; Peddis, D.; Casu, M.; Sanna, R.; Angius, F.; Diaz, G.; Piccaluga, G. *Chem. Mater.* **2010**, *22*, 3353.
- (17) Wang, L.; Wang, X.; Luo, J.; Wanjala, B. N.; Wang, C.; Chernova, N. A.; Engelhard, M. H.; Liu, Y.; Bae, I.; Zhong, C. *J. Am. Chem. Soc.* **2010**, *132*, 17686.
- (18) Chinnasamy, C. N.; Jeyadevan, B.; Shinoda, K.; Tohji, K.; Djayaprawira, D. J.; Takahashi, M.; Joseyphus, R. J.; Narayanasamy, A. *Appl. Phys. Lett.* **2003**, *83*, 2862.
- (19) Gurgel, A. L.; Soares, J. M.; Chaves, D. S.; Chaves, D. S.; Xavier, M. M. Jr.; Morales, M. A.; Baggio-Saitovitch, E. M. *J. App. Phys.* **2010**, *107*, 09A746 1–3.
- (20) *Introduction to X-ray Powder Diffractometry*; Jenkins, R., Snyder, R. L., Eds.; Wiley: New York, 1996.
- (21) Lima, E. Jr.; Vargas, J. M.; Zysler, R. D.; Rechenberg, H. R.; Cohen, R.; Arbiol, J.; Goya, G. F.; Ibarra, A.; Ibarra, M. R. *Nanotechnology* **2009**, *20*, 045606.
- (22) Ong, Q. K.; Wei, A.; Lin, X.-M. *Phys. Rev. B* **2009**, *80*, 134418.
- (23) Molina Concha, B.; De Biasi, E.; Zysler, R. D. *Phys. B* **2008**, *403*, 390.
- (24) Goodenough, J. B. *Prog. Solid State Chem.* **1971**, *5*, 145.
- (25) Nogués, J.; Schuller, I. K. *J. Magn. Magn. Mater.* **1999**, *192*, 203.

- (26) Golosovsky, I. V.; Mirebeau, I.; Sakhnenko, V. P.; Kurdyukov, D. A.; Kumzerov, Y. A. *Phys. Rev. B* **2005**, *72*, 144409.
- (27) Tang, Z. X.; Sorensen, C. M.; Klabunde, K. J.; Hadjipanayis, G. C. *Phys. Rev. Lett.* **1991**, *67*, 3602.
- (28) Ponpandian, N.; Narayanasamy, A.; Chinnasamy, C. N.; Sivakumar, N.; Greeneche, J.-M.; Chattopadhyay, K.; Shinoda, K.; Jeyadevan, B.; Tohji, K. *Appl. Phys. Lett.* **2005**, *86*, 192510.
- (29) Yang, A.; Chinnasamy, C. N.; Greeneche, J. M.; Chen, Y. J.; Yoon, S. D.; Chen, Z. H.; Hsu, K. L.; Cai, Z. H.; Ziemer, K.; Vittoria, C.; Harris, V. G. *Nanotechnology* **2009**, *20*, 185704.
- (30) Wesselinowa, J. M. *J. Magn. Magn. Mater.* **2010**, *322*, 234.
- (31) Arelaro, A. D.; Lima, E. Jr.; Rossi, L. M.; Kiyohara, P. K.; Rechenberg, H. R. *J. Magn. Magn. Mater.* **2008**, *320*, e335.
- (32) Nogués, J.; Sort, J.; Langlais, V.; Skumryev, V.; Suriñach, S.; Muñoz, J. S.; Baró, M. D. *Phys. Rep.* **2005**, *422*, 65.
- (33) Kanamori, J. *Prog. Theor. Phys.* **1957**, *17*, 197.
- (34) Meiklejohn, W. H.; Been, C. P. *Phys. Rev. B* **1957**, *105*, 904.
- (35) Tracy, J. B.; Weiss, D. N.; Dinega, D. P.; Bawendi, M. G. *Phys. Rev. B* **2005**, *72*, 064404.